Submitted to ADVANCED MATERIALS

DOI: 10.1002/adma.201401228

Layer-by-layer Assembled Heteroatom-Doped Graphene Films with Ultrahigh Volumetric Capacitance and Rate Capability for Micro-Supercapacitors

By Zhong-Shuai Wu, Khaled Parvez, Andreas Winter, Henning Vieker, Xianjie Liu, Sheng Han, Andrey Turchanin, Xinliang Feng,* and Klaus Müllen*

[*] Dr. Z.S. Wu, Mr. K. Parvez, Prof. Dr. X. L. Feng, Prof. Dr. K. Müllen

Max-Planck-Institut für Polymerforschung

Ackermannweg 10, 55128 Mainz (Germany)

E-mail: feng@mpip-mainz.mpg.de; muellen@mpip-mainz.mpg.de

Mr. A. Winter, Mr. H. Vieker, PD Dr. A. Turchanin

Faculty of Physics, University of Bielefeld,

Universitätsstr. 25, 33615 Bielefeld, Germany

Dr. X.J. Liu

Department of Physics, Chemistry and Biology, Linköping University, SE-58183 Linköping, Sweden

Dr. S. Han, Prof. Dr. X. L. Feng

School of Chemistry and Chemical Engineering, Shanghai Jiao Tong University,

200240, Shanghai, P. R. China

Keywords: Layer-by-layer Self-assembly, Heteroatom Doping, Graphene Film, Energy Storage, Micro-Supercapacitors

The rapid development of miniaturized, wearable, and portable electronics have made micro-power sources on chips an important prerequisite.[1-5] In this regard, planar micro-supercapacitors (MSCs) with short ion diffusion distances are considered to be highly competitive candidates for integrating numerous electronic devices due to their ultrahigh power density, large rate capability, and superior cycling lifetime.[6-9] Since 2003, when Sung *et al.* reported the first prototype planar MSCs based on conducting polymers,[10] tremendous

attention has been focused on planar MSCs, for which a series of pseudocapacitive electrode materials, such as RuO_2,[11] MnO_2,[12] VS_2,[13] and polyaniline,[14, 15] has been used. These state-of-the-art pseudocapacitve MSCs deliver a high volumetric capacitance, but generally exhibit low power density and a slow frequency response. To overcome these limitations, carbon-based MSCs utilizing activated carbon,[16, 17] carbide-derived carbon,[3, 18] onion-like carbon,[2] carbon nanotubes (CNTs),[19, 20] and graphene[7, 8] were developed.

Graphene-based materials, such as reduced graphene oxide,[21] CVD graphene,[22] chemically-reduced graphene,[7, 8, 23] graphene quantum dots,[24, 25] and nanohybrids of graphene/CNTs,[26, 27] graphene/polyaniline,[28] and graphene/MnO_2,[29] were recently exploited as advanced electrodes for planar MSCs by taking advantage of the planar device geometry and the unique structure of graphene for charge storage.[22, 30-33] In particular, graphene-based thin films for MSCs have attracted attention due to their polymer binder-free process, low macropore volume, and good adhesion between the current collector and active material,[7, 8, 23] which are essential features for achieving the high volumetric capacitance of MSCs.[34, 35] For the development of next-generation graphene-based MSCs, graphene doping with heteroatoms (e.g., N, B, S, or P) is a promising strategy to enhance the performance of supercapacitors by the introduction of pseudocapacitance.[36-38] Despite the successful preparation of heteroatom-doped graphene sheets and porous graphene materials for supercapacitors, the fabrication of doped graphene films with a controlled thickness and uniform co-doping of different heteroatoms has not yet been reported.

Here we describe the development of large-area, highly uniform, ultrathin, nitrogen and boron co-doped graphene (BNG) films for high-performance MSCs. The BNG film was prepared using a layer-by-layer (LBL) assembly of anionic graphene oxide (GO) nanosheets and cationic poly-L-Lysine (PLL) as a nitrogen-containing precursor, followed by intercalation of H_3BO_3 within the layers and annealing treatment (Fig.1a-f). The PLL and H_3BO_3 incorporated into the assembled multilayer films not only serve as nitrogen- and

boron-rich precursors, respectively, but also generate micropore fillers to promote the formation of porous, yet densely packed BNG films during the thermal treatment. All-solid-state planar MSCs were manufactured by lithographically dry-etching the as-produced BNG films on silicon wafers (Fig.1f-h), providing a pronounced pseudocapacitive behavior with ultrahigh volumetric capacitance (~488 F/cm^3). This is the highest value reported to date for graphene-based supercapacitors, and an ultrahigh operation scan rate of up to 2000 V/s.

The LBL assembly is a simple and versatile bottom-up method to produce ultrathin multilayer films with a controlled thickness ranging from the nanometer to micrometer-scale through sequential immersion of a substrate into aqueous solution with pre-charged functional materials and repeated self-assembly.[39-45] In our work, PLL with positively-charged amino acids (Fig.S1 in Supporting Information) was chosen to control the deposition of negatively-charged GO nanosheets onto a surface by electrostatic attraction. Figure 1a-e illustrates the fabrication of $(PLL/GO)_n$ multi-layer films. The Si/SiO_2 wafer was initially treated by oxygen plasma to make the surface hydrophilic, and then the PLL and GO layers were repeatedly adsorbed on the modified silicon wafer to yield the multilayer $(PLL/GO)_n$ ($n \leq 10$) films.

The surface topography of the $(PLL/GO)_n$ film was examined by atomic force microscopy (AFM) and scanning electron microscopy (SEM) measurements (Fig.2a-c, Figs.S2-S4). A $(PLL/GO)_1$ film on a silicon substrate was almost completely covered by individual monolayer GO nanosheets with a thickness of ~1.2 nm (Fig.S2), and only a few overlapped GO nanosheets were restacked at their edges (Fig.2a). A total coverage of more than 90% was estimated for the first-layer deposited film, suggesting a highly efficient assembly of GO with PLL. The surface was fully covered by GO nanosheets after two rounds of assembly, as evidenced by the AFM and SEM visualizations (Fig.2b,c). Thus, large-area continuous $(PLL/GO)_n$ films with a desirable layer number were subsequently achieved with PLL and GO nanosheets deposited in an alternating fashion (Fig.S3). Notably, the resulting $(PLL/GO)_n$ films had a low surface roughness (≤1 nm) for the entire measurement area (Fig.S4). It should

be mentioned that the assembling regularity of each layer, e.g., PLL layer and GO layer studied by AFM height images and 3D surface plots reveal the intimate interaction of both negative-charged GO and positively-charged PLL species during the LBL assembly process (Figs.S5 and S6), which is critical for efficient self-assmebly.

The structural changes of the $(PLL/GO)_{10}$ film and H_3BO_3-intercalated $(PLL/GO)_{10}$ film were investigated based on their X-ray diffraction (XRD) patterns. As shown in Fig. 3a, the XRD pattern of a $(PLL/GO)_{10}$ film exhibited a sharp diffraction peak (002) at 8.3°, corresponding to a d-spacing of 10.6 Å, which is larger than that of spin-coated GO film (8.9 Å) without the incorporation of PLL layers.[7] With H_3BO_3 intercalation, the characteristic (002) peak shifts to a lower angle of 7.6°, with a larger d-spacing of 11.6 Å. In addition, a notable peak at 27.8° was oberved, indicative of the presence of the H_3BO_3 (JCPDS 73-2158) in the assembled multilayer films.

Thermal treatment at 800°C for 30 min in nitrogen atmosphere was subsequently performed to convert the H_3BO_3-intercalated $(PLL/GO)_{10}$ film into a BNG film and the $(PLL/GO)_{10}$ film into a nitrogen-doped graphene (NG) film. The color changed from olive green to dark green, indicating the formation of graphene films (Fig.S7). Figure 2d-i shows the AFM and SEM images of the BNG and NG films, which exhibit a smooth surface morphology with good continuity and uniformity (Fig.2d,g, Fig.S8). Only small wrinkles with a submicrometer size formed on the top surface of the BNG film (Fig.2e,f) and NG film (Fig.2h,i). A detailed comparison of the thickness of $(PLL/GO)_n$ films before and after thermal annealing is presented in Figure S9. The decreased thickness of the film after heat treatment can be attributed to the removal of oxygen-containing groups on GO and decomposition of the PLL (and H_3BO_3) precursor within the graphene nanosheets (Fig.S10).

XRD patterns (Fig. 3a) after thermal annealing revealed the (002) diffraction peak of both NG and BNG films at around 25.8°, with a d-spacing of 3.45 Å. This value is slightly larger than that of graphite (3.35 Å), and is likely due to the decomposition of PLL (and H_3BO_3)

incorporated as micropore fillers and the residual oxygenated groups on GO remaining between the layers.

The Raman spectra showed broad D and G bands, located at 1349 and 1600 cm^{-1} for $(PLL/GO)_{10}$ film, 1347 and 1586 cm^{-1} for H_3BO_3-intercalated $(PLL/GO)_{10}$ film, 1361 and 1593 cm^{-1} for NG film, and 1359 and 1589 cm^{-1} for BNG film, respectively (Fig. 3b). The I_D/I_G ratio increased from 0.89 for $(PLL/GO)_{10}$ film to 1.01 for NG film, and from 0.99 for H_3BO_3-intercalated $(PLL/GO)_{10}$ film to 1.12 for BNG film. The increased I_D/I_G ratio for NG and BNG after thermal treatment can be attributed to the heteroatom doping that produces new defective sites in the sp^2 carbon frameworks. [46-49]

X-ray photoelectron spectroscopy (XPS) was used to probe the chemical composition of the BNG and NG films (Fig.3c,d, Fig.S11). The BNG film exhibited a doping content of 3.1 at % for nitrogen and 3.6 at % for boron, respectively. NG film also showed a comparable nitrogen doping content of 3.1 at %. Given that the $(PLL/GO)_{10}$ film contained only ~3.6 at % nitrogen moieties, the doping level of heteroatoms for BNG and NG films achieved after thermal annealing is quite remarkable. This result suggests that confinement of nitrogen and boron precursors within the assembled GO films is responsible for the efficient doping process. High-resolution C1s XPS spectra revealed that the intensities of oxygen-containing groups at 286.6 (C-O), 287.3 (C=O), and 288.2 eV (O=C-O) dramatically decreased and new bonds (like C-N, N-C=O) appeared after annealing (Fig.S11).[50, 51] The C/O ratios of ~13.3 for NG film and ~11.8 for BNG film confirmed the restoration of the sp^2-hybridized carbon lattices. The N1s XPS spectrum of $(PLL/GO)_{10}$ film can be fitted to two distinct peaks at 399.5 and 401.3 eV (Fig. 2d), which originate from the C-N (N-C=O) and NH_3^+ groups of PLL, respectively.[52] After thermal annealing, the high-resolution N1s scan of NG film indicated the presence of multiple forms of nitrogen-containing moieties, that is, pyridinic N (398.3±0.1 eV), graphitic N (401.3±0.1 eV), and NO_2 (405.3±0.1 eV).[46, 53-55] For the BNG film, a new C-B-N peak (399.2 eV) was clearly identified in the N1s spectrum.[47] In the B1s

XPS spectrum for BNG film (inset in Fig.3c), three bonds of B-C (189.0 eV), B-N (191.5 eV) and B-O (192.8 eV) can be unraveled.[56-58] Energy dispersive X-ray (EDX) spectra and mapping analysis further confirmed the uniform co-doping of the nitrogen and boron moieties into the BNG film (Fig.S12). The measured electrical conductivity of BNG and NG films was ~230 and ~276 S/cm, respectively, highlighting the efficient reduction of the graphene films.

Next, all-solid-state planar MSCs were fabricated based on doped graphene films (Fig.4a). The fabrication scheme of the MSCs is presented in Figure 1f-g, which includes lithographic micro-patterns and deposition of a gold layer on the surface of BNG or NG film, oxygen plasma etching for removal of the exposed graphene area, drop-casting of the H_2SO_4/polyvinyl alcohol (H_2SO_4/PVA) gel electrolyte,[47] and solidification of the gel electrolyte. The corresponding MSCs based on BNG and NG films were named BNG-MSCs and NG-MSCs, respectively (see details in Supporting Information). SEM and AFM images of the patterned BNG films revealed a relatively smooth edge along the fingers (Fig. 4b-d).

The electrochemical performance of BNG-MSCs and NG-MSCs was first examined by cyclic voltammetry (CV) at scan rates ranging from 0.01 to 2000 V s^{-1} (Fig.4e-k). To highlight the critical role of heteroatom doping, we also fabricated planar MSCs based on reduced graphene (RG) film (denoted RG-MSCs, thickness ~8.0 nm) without heteroatom doping. The CV curves of RG-MSCs are shown in Fig.4e-k for comparison. At low scan rates from 10 to 100 mV/s (Fig.4e, g), both BNG-MSCs and NG-MSCs exhibited a large capacitive response, accompanied by strong redox peaks, indicative of the presence of a pseudocapacitive effect with heteroatom-doping.[47] In contrast, RG-MSCs exhibited a typical electric double-layer capacitive behaviour with a nearly rectangular CV shape.[59-61] Furthermore, BNG-MSCs had a greater capacitive response than NG-MSCs, suggesting that boron and nitrogen have synergistic doping effects.[47, 62] At a high scan rate, BNG-MSCs also had a larger integration area (Fig.4g-k) and higher discharge current (Fig. 4l) than NG-MSCs and RG-MSCs, confirming that co-doping indeed greatly improved the capacitive

performance.[47, 62] Remarkably, BNG-MSCs allowed for operation at an ultrahigh scan rate of up to 2000 V s^{-1} (Fig. 4k,l), which is three orders of magnitude higher than that of conventional supercapacitors and represents the highest value for a high-power MSCs reported to date (Table S1).

The volumetric capacitance of BNG, NG, and RG films for MSCs as a function of scan rate is compared in Figure 5a. Notably, the volumetric capacitance of BNG film for MSCs recorded at 10 mV/s was ~488 F/cm^3, higher than that of NG (~425 F/cm^3) and much higher than that of RG (~245 F/cm^3). The enhanced performance of the BNG-MSCs is likely due to the following: (1) co-doping with dual heteroatoms probably creates new electrochemically active moieties (e.g., B-N-C) with a synergistic effect that provides additional pseudocapacitance contributions;[47-49, 63] and (2) the new binding environment of neighboring B and N atoms directly incorporated into the graphene lattice is favorable for improving the interface wettability of the electrode with the electrolyte, resulting in a thickened electrochemical double layer.[47, 57, 62]

The energy and power densities were estimated on the basis of the CV measurements of MSCs (Fig.5b). Based on the above-described volumetric capacitance and working voltage (1.0 V), the energy density $E_{electrode}$ and power density $P_{electrode}$ were calculated to be ~16.9 mWh/cm^3 and ~4560 W/cm^3 for BNG film, values higher than those of a NG film (14.7 mWh/cm^3 and 3960 W/cm^3) and a RG film (8.5 mWh/cm^3 and 3220 W/cm^3). By taking into account the whole volume of a packaged MSC,[2, 3, 7] a remarkable energy density E_{device} of ~3.4 mWh/cm^3 for BNG-MSCs was achieved, comparable to that of high-energy lithium thin-film batteries (1~10 mWh/cm^3).[2] More importantly, BNG-MSCs delivered a maximum power density P_{device} of ~910 W/cm^3, which is much higher than that of reported MSCs (~495 W/cm^3, Table S1),[7] and comparable to that of high-power electrolytic capacitors (10^1~10^3 W/cm^3).[31] The cycling stability of BNG-MSCs was demonstrated for 100000 cycles at a scan

rate of 500 V s^{-1} (Fig.5c,d). The CV shapes (Fig.5c) and ~95.2% of the initial capacitance were maintained (Fig.5d), indicating the superior cycling stability.

In summary, we demonstrated an efficient LBL self-assembly and intercalation protocol for constructing large-area, ultrathin, uniform heteroatom-doped graphene films. The fabricated MSCs based on a boron and nitrogen co-doped graphene film exhibited a remarkable pseudocapacitve behavior with an ultrahigh volumetric capacitance of ~488 F/cm^3, and an outstanding rate capability of up to 2000 V/s. The described LbL fabrication provides the opportunity to incorporate metal or metal oxide nanostructures into doped-graphene films, which hold great potential for other thin-film energy storage and conversion devices, such as metal-free electrocalatysts for oxygen reduction reactions in fuel cells[54] and lithium battery applications.[64]

Supporting Information

Supporting Information is available online from the Wiley Online Library or from the author.

The authors thank G. Glaßer for the kind help with SEM and EXD measurements.

Acknowledgements

This work was financially supported by the ERC Grant on 2DMATER and NANOGRAPH, EU Project GENIUS and MoQuas, DFG SPP 1459 and Heisenberg Programme, and EC under Graphene Flagship (No. CNECT-ICT-604391).

Received: ((will be filled in by the editorial staff))
Revised: ((will be filled in by the editorial staff))
Published online: ((will be filled in by the editorial staff))

References

[1] D. R. Rolison, R. W. Long, J. C. Lytle, A. E. Fischer, C. P. Rhodes, T. M. McEvoy, M. E. Bourga, A. M. Lubers, *Chem. Soc. Rev.* **2009**, *38*, 226.

[2] D. Pech, M. Brunet, H. Durou, P. H. Huang, V. Mochalin, Y. Gogotsi, P. L. Taberna, P. Simon, *Nat. Nanotechnol.* **2010**, *5*, 651.

[3] J. Chmiola, C. Largeot, P. L. Taberna, P. Simon, Y. Gogotsi, *Science* **2010**, *328*, 480.

[4] J. H. Pikul, H. G. Zhang, J. Cho, P. V. Braun, W. P. King, *Nat. Commun.* **2013**, *4*, 1732.

[5] Z. S. Wu, X. L. Feng, H. M. Cheng, *Natl. Sci. Rev.* **2014**, DOI: 10.1093/nsr/nwt003.

[6] J. H. Sung, S. J. Kim, S. H. Jeong, E. H. Kim, K. H. Lee, *J. Power Sources* **2006**, *162*, 1467.

[7] Z. S. Wu, K. Parvez, X. L. Feng, K. Müllen, *Nat. Commun.* **2013**, *4*, 2487.

[8] M. F. EI-Kady, R. B. Kaner, *Nat. Commun.* **2013**, *4*, 1475.

[9] M. Beidaghi, Y. Gogotsi, *Energy Environ. Sci.* **2014**, DOI: 10.1039/c3ee43526a.

[10] J. H. Sung, S. J. Kim, K. H. Lee, *J. Power Sources* **2003**, *124*, 343.

[11] S. Makino, Y. Yamauchi, W. Sugimoto, *J. Power Sources* **2013**, *227*, 153.

[12] M. Q. Xue, Z. Xie, L. S. Zhang, X. L. Ma, X. L. Wu, Y. G. Guo, W. G. Song, Z. B. Li, T. B. Cao, *Nanoscale* **2011**, *3*, 2703.

[13] J. Feng, X. Sun, C. Z. Wu, L. L. Peng, C. W. Lin, S. L. Hu, J. L. Yang, Y. Xie, *J. Am. Chem. Soc.* **2011**, *133*, 17832.

[14] W. W. Liu, X. B. Yan, J. T. Chen, Y. Q. Feng, Q. J. Xue, *Nanoscale* **2013**, *5*, 6053.

[15] C. Meng, J. Maeng, S. W. M. John, P. P. Irazoqui, *Adv. Energy Mater.* **2014**, DOI:10.1002/aenm.201301269.

[16] H. Durou, D. Pech, D. Colin, P. Simon, P. L. Taberna, M. Brunet, *Microsyst. Technol.* **2012**, *18*, 467.

[17] D. Pech, M. Brunet, P. L. Taberna, P. Simon, N. Fabre, F. Mesnilgrente, V. Conedera, H. Durou, *J. Power Sources* **2010**, *195*, 1266.

[18] P. Huang, M. Heon, D. Pech, M. Brunet, P. L. Taberna, Y. Gogotsi, S. Lofland, J. D. Hettinger, P. Simon, *J. Power Sources* **2013**, *225*, 240.

[19] H. J. Ahn, W. B. Kim, T. Y. Seong, *Electrochem Commun* **2008**, *10*, 1284.

[20] D. Kim, G. Shin, Y. J. Kang, W. Kim, J. S. Ha, *ACS Nano* **2013**, *7*, 7975.

[21] W. Gao, N. Singh, L. Song, Z. Liu, A. L. M. Reddy, L. J. Ci, R. Vajtai, Q. Zhang, B. Q. Wei, P. M. Ajayan, *Nat. Nanotechnol.* **2011**, *6*, 496.

[22] J. J. Yoo, K. Balakrishnan, J. S. Huang, V. Meunier, B. G. Sumpter, A. Srivastava, M. Conway, A. L. M. Reddy, J. Yu, R. Vajtai, P. M. Ajayan, *Nano Lett.* **2011**, *11*, 1423.

[23] Z. Q. Niu, L. Zhang, L. L. Liu, B. W. Zhu, H. B. Dong, X. D. Chen, *Adv. Mater.* **2013**, *25*, 4035.

[24] W. W. Liu, Y. Q. Feng, X. B. Yan, J. T. Chen, Q. J. Xue, *Adv. Funct. Mater.* **2013**, *23*, 4111.

[25] W. W. Liu, X. B. Yan, J. T. Chen, Y. Q. Feng, Q. J. Xue, *Nanoscale* **2013**, *5*, 6053.

[26] M. Beidaghi, C. L. Wang, *Adv. Funct. Mater.* **2012**, *22*, 4501.

[27] J. Lin, C. G. Zhang, Z. Yan, Y. Zhu, Z. W. Peng, R. H. Hauge, D. Natelson, J. M. Tour, *Nano Lett.* **2013**, *13*, 72.

[28] M. A. Q. Xue, F. W. Li, J. Zhu, H. Song, M. N. Zhang, T. B. Cao, *Adv. Funct. Mater.* **2012**, *22*, 1284.

[29] L. L. Peng, X. Peng, B. R. Liu, C. Z. Wu, Y. Xie, G. H. Yu, *Nano Lett.* **2013**, *13*, 2151.

[30] D. Pech, M. Brunet, T. M. Dinh, K. Armstrong, J. Gaudet, D. Guay, *J. Power Sources* **2013**, *230*, 230.

[31] M. F. El-Kady, V. Strong, S. Dubin, R. B. Kaner, *Science* **2012**, *335*, 1326.

[32] X. W. Yang, C. Cheng, Y. F. Wang, L. Qiu, D. Li, *Science* **2013**, *341*, 534.

[33] Z. S. Wu, G. M. Zhou, L. C. Yin, W. C. Ren, F. Li, H. M. Cheng, *Nano Energy* **2012**, *1*, 107.

[34] M. Heon, S. Lofland, J. Applegate, R. Nolte, E. Cortes, J. D. Hettinger, P. L. Taberna, P. Simon, P. H. Huang, M. Brunet, Y. Gogotsi, *Energy Environ. Sci.* **2011**, *4*, 135.

[35] M. R. Lukatskaya, O. Mashtalir, C. E. Ren, Y. Dall'Agnese, P. Rozier, P. L. Taberna, M. Naguib, P. Simon, M. W. Barsoum, Y. Gogotsi, *Science* **2013**, *341*, 1502.

[36] R. L. Liu, X. L. Feng, D. Q. Wu, K. Müllen, *Angew. Chem. Int. Ed.* **2010**, *49*, 2565.

[37] L. Z. Fan, L. Zhao, M. Q. Zhou, H. Guan, S. Y. Qiao, M. Antonietti, M. M. Titirici, *Adv. Mater.* **2010**, *22*, 5202.

[38] H. M. Jeong, J. W. Lee, W. H. Shin, Y. J. Choi, H. J. Shin, J. K. Kang, J. W. Choi, *Nano Lett.* **2011**, *11*, 2472.

[39] K. Ariga, J. P. Hill, Q. M. Ji, *Phys. Chem. Chem. Phys.* **2007**, *9*, 2319.

[40] H. L. Li, S. P. Pang, S. Wu, X. L. Feng, K. Mullen, C. Bubeck, *J. Am. Chem. Soc.* **2011**, *133*, 9423.

[41] S. T. Han, Y. Zhou, C. D. Wang, L. F. He, W. J. Zhang, V. A. L. Roy, *Adv. Mater.* **2013**, *25*, 872.

[42] Q. M. Ji, I. Honma, S. M. Paek, M. Akada, J. P. Hill, A. Vinu, K. Ariga, *Angew. Chem. Int. Ed.* **2010**, *49*, 9737.

[43] S. W. Lee, B. S. Kim, S. Chen, Y. Shao-Horn, P. T. Hammond, *J. Am. Chem. Soc.* **2009**, *131*, 671.

[44] K. Ariga, Y. Yamauchi, G. Rydzek, Q. Ji, Y. Yonamine, K. C. W. Wu, J. P. Hill, *Chem. Lett.* **2014**, *43*, 36.

[45] N. Joseph, P. Ahmadiannamini, R. Hoogenboom, I. F. J. Vankelecom, *Polym. Chem.* **2014**, *5*, 1817.

[46] Z. S. Wu, W. C. Ren, L. Xu, F. Li, H. M. Cheng, *ACS Nano* **2011**, *5*, 5463.

[47] Z. S. Wu, A. Winter, L. Chen, Y. Sun, A. Turchanin, X. Feng, K. Müllen, *Adv. Mater.* **2012**, *24*, 5130.

[48] S. Wang, E. Iyyamperumal, A. Roy, Y. Xue, D. Yu, L. M. Dai, *Angew. Chem. Int. Ed.* **2011**, *50*, 11756.

[49] S. Y. Wang, L. P. Zhang, Z. H. Xia, A. Roy, D. W. Chang, J. B. Baek, L. M. Dai, *Angew. Chem. Int. Ed.* **2012**, *51*, 4209.

[50] Z. S. Wu, W. Ren, L. Gao, B. Liu, C. Jiang, H. M. Cheng, *Carbon* **2009**, *47*, 493.

[51] S. W. Lee, N. Yabuuchi, B. M. Gallant, S. Chen, B. S. Kim, P. T. Hammond, Y. Shao-Horn, *Nat. Nanotechnol.* **2010**, *5*, 531.

[52] E. P. Ivanova, D. K. Pham, G. M. Demyashev, D. V. Nicolau, *Proceedings of SPIE* **2002**, *4937*, 23.

[53] X. L. Li, H. L. Wang, J. T. Robinson, H. Sanchez, G. Diankov, H. J. Dai, *J. Am. Chem. Soc.* **2009**, *131*, 15939.

[54] L. T. Qu, Y. Liu, J. B. Baek, L. M. Dai, *ACS Nano* **2010**, *4*, 1321.

[55] Z. S. Wu, S. B. Yang, Y. Sun, K. Parvez, X. L. Feng, K. Müllen, *J. Am. Chem. Soc.* **2012**, *134*, 9082.

[56] L. S. Panchokarla, K. S. Subrahmanyam, S. K. Saha, A. Govindaraj, H. R. Krishnamurthy, U. V. Waghmare, C. N. R. Rao, *Adv. Mater.* **2009**, *21*, 4726.

[57] B. H. Kim, K. S. Yang, H. G. Woo, *Mater. Lett.* **2013**, *93*, 190.

[58] J. S. Park, J. M. Lee, S. K. Hwang, S. H. Lee, H.-J. Lee, B. R. Lee, H. I. Park, J.-S. Kim, S. Yoo, M. H. Song, S. O. Kim, *J. Mater. Chem.* **2012**, *22*, 12695.

[59] D. W. Wang, F. Li, M. Liu, G. Q. Lu, H. M. Cheng, *Angew. Chem. Int. Ed.* **2008**, *47*, 373.

[60] Z. S. Wu, D. W. Wang, W. Ren, J. Zhao, G. Zhou, F. Li, H. M. Cheng, *Adv. Funct. Mater.* **2010**, *20*, 3595.

[61] Z. S. Wu, Y. Sun, Y. Z. Tan, S. B. Yang, X. L. Feng, K. Müllen, *J. Am. Chem. Soc.* **2012**, *134*, 19532−19535.

[62] H. L. Guo, Q. M. Gao, *J. Power Sources* **2009**, *186*, 551.

[63] E. Iyyamperumal, S. Y. Wang, L. M. Dai, *ACS Nano* **2012**, *6*, 5259.

[64] A. L. M. Reddy, A. Srivastava, S. R. Gowda, H. Gullapalli, M. Dubey, P. M. Ajayan, *ACS Nano* **2010**, *4*, 6337.

Figures and Figure Caption

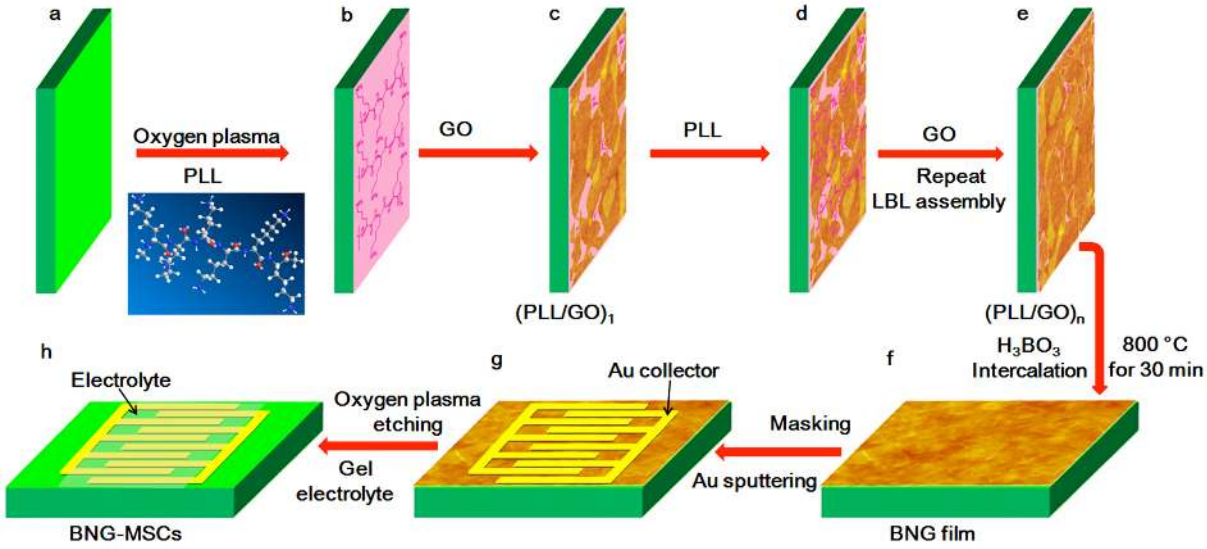

Figure 1. Schematic illustration of LBL-assembled heteroatom-doped films for planar MSCs on a Si/SiO_2 wafer. (a) Electrostatic adsorption of cationic PLL on the hydrophilic surface of silicon treated with an oxygen plasma. Inset: molecular structure of PLL with 6 units (red: N in $–NH_3^+$; blue: N in –NH–; gray: C; white: H) (b) LBL assembly of anionic GO nanosheets on a PLL-adsorbed silicon wafer. (c, d) Repeated self-assembly of PLL and GO nanosheets into $(PLL/GO)_n$ ultrathin films. (e) H_3BO_3 intercalation and annealing treatment to convert a $(PLL/GO)_n$ film into a BNG film. (f) Lithographic micro-patterns and deposition of a gold current collector through a homemade mask. (g) Oxygen plasma etching and drop-casting of gel electrolyte on interdigital fingers. (h) All-solid-state BNG-MSCs obtained after solidification of gel electrolyte.

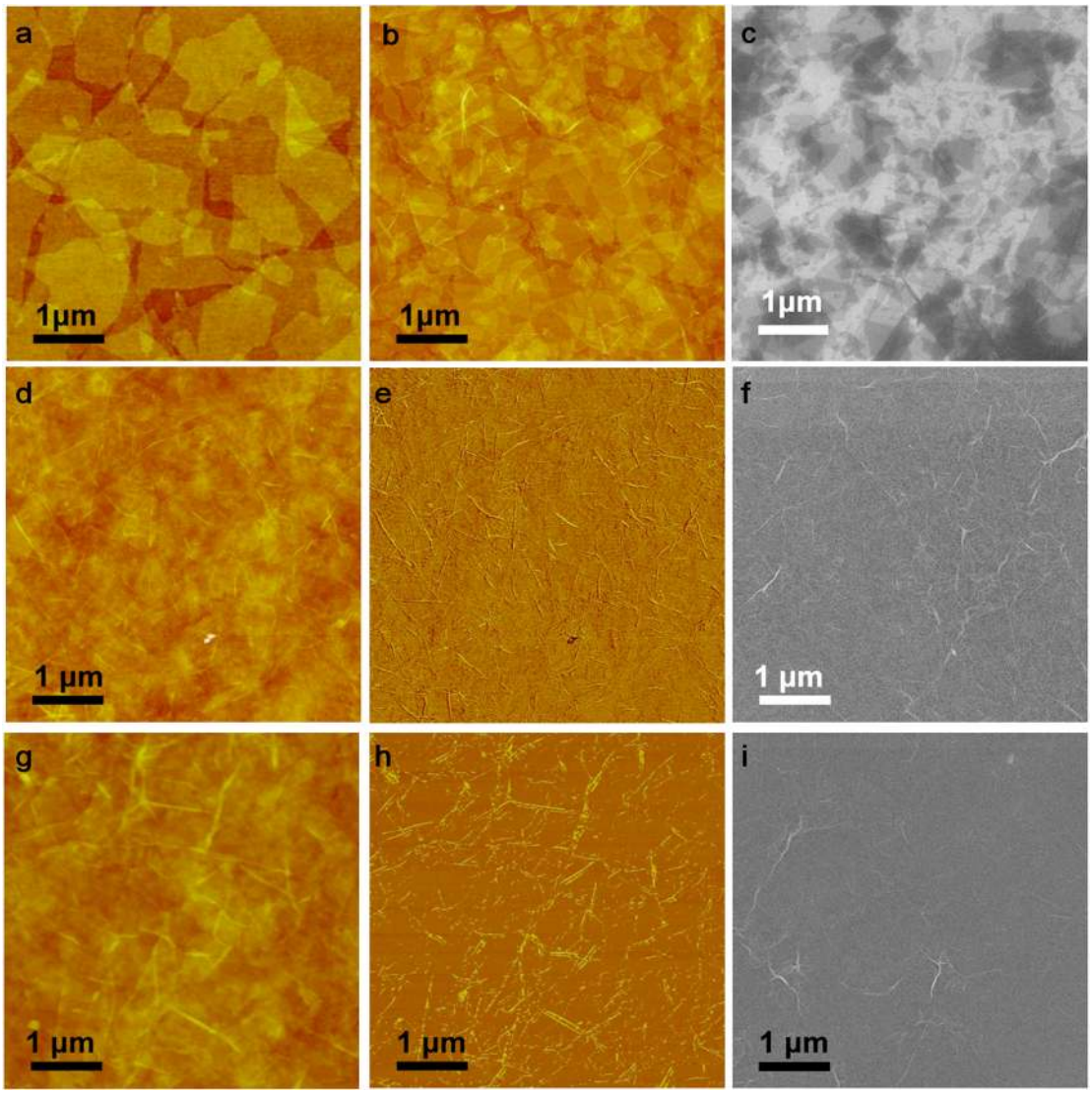

Figure 2. Surface morphology of LBL-assembled $(PLL/GO)_n$, NG, and BNG films. (a,b) AFM image of (a) $(PLL/GO)_1$ film. (b) AFM and (c) SEM images of $(PLL/GO)_2$ film. (d) AFM height image, (e) AFM phase image, and (f) SEM image of NG film annealed from $(PLL/GO)_{10}$. (g) AFM height image, (h) AFM phase image and (i) SEM image of a BNG film annealed from H_3BO_3-intercalated $(PLL/GO)_{10}$.

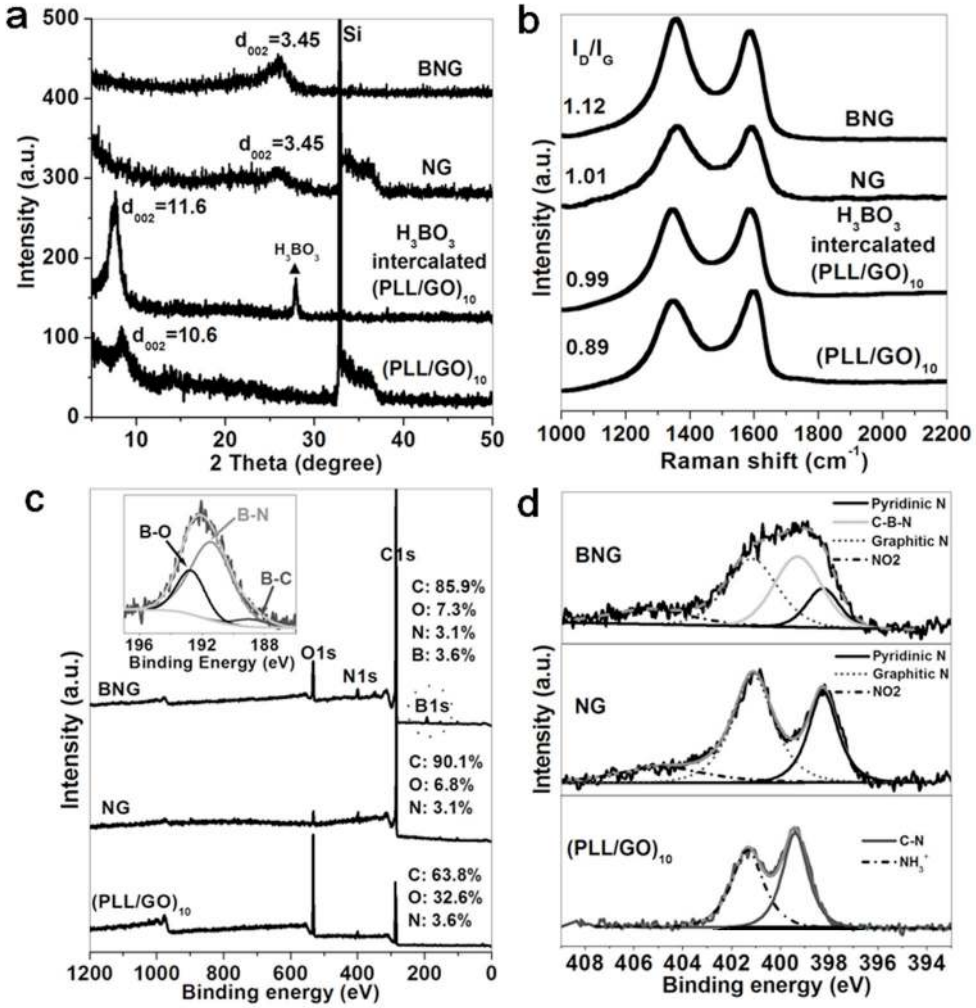

Figure 3. Structural characterization of BNG, NG, H_3BO_3-intercalated $(PLL/GO)_{10}$, and $(PLL/GO)_{10}$ films. (a) XRD patterns, (b) Raman spectra of BNG, NG, H_3BO_3-intercalated $(PLL/GO)_{10}$, and $(PLL/GO)_{10}$. (c) Overview XPS spectra (Inset: B1s XPS of BNG film) and (d) high-resolution N1s XPS spectra of BNG, NG, and $(PLL/GO)_{10}$ films.

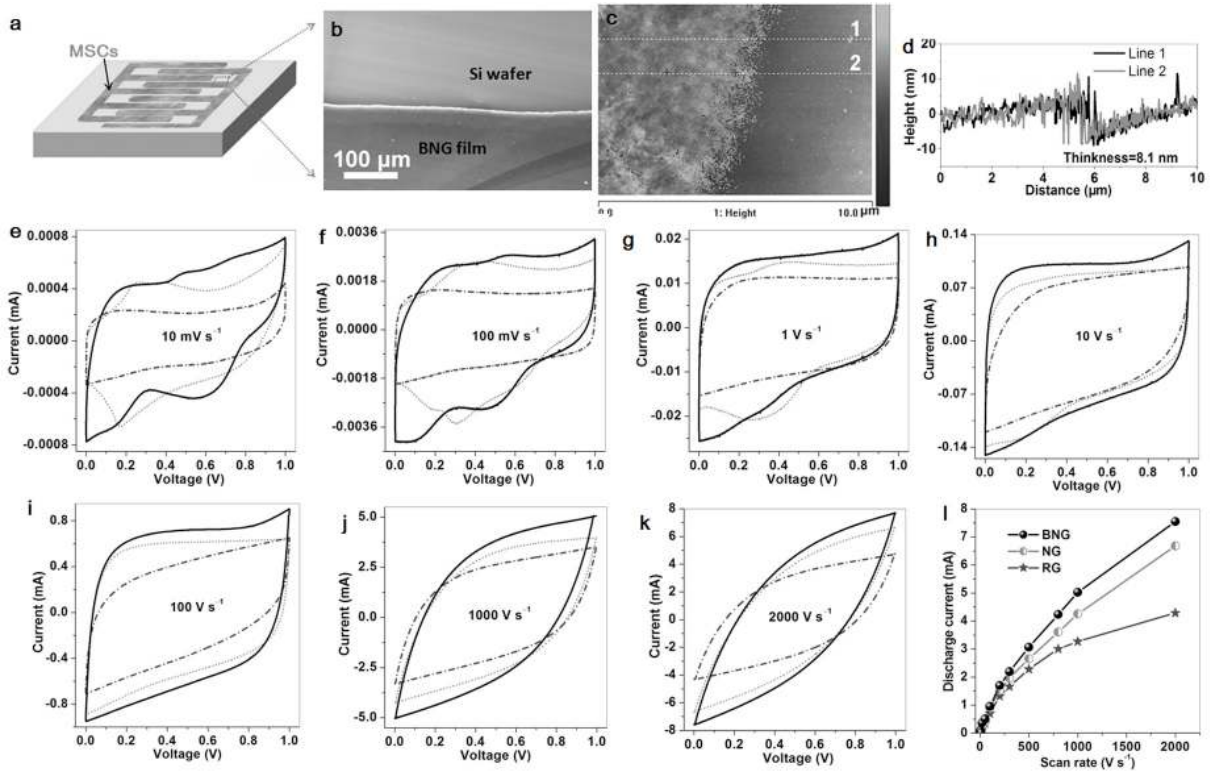

Figure 4. Electrochemical comparison of BNG-MSCs, NG-MSCs, and RG-MSCs. (a) Scheme of all-solid-state BNG-MSCs on a silicon wafer. (b) SEM image of the finger edge of a BNG film. (c) AFM image and (d) height profile of a BNG film (with a thickness of ~8.1 nm) annealed from a H_3BO_3-intercalated $(PLL/GO)_{10}$ film. (e-k) CV curves of BNG-MSCs (black lines), NG-MSCs (gray, short dot lines), and RG-MSCs (dark gray, short dash dot lines) obtained at different scan rates of (e) 0.01, (f) 0.1, (g) 1, (h) 10, (i) 100, (g) 1000, and (k) 2000 V s^{-1}. (l) Plot of the discharge current as a function of the scan rate for BNG-MSCs, NG-MSCs, and RG-MSCs.

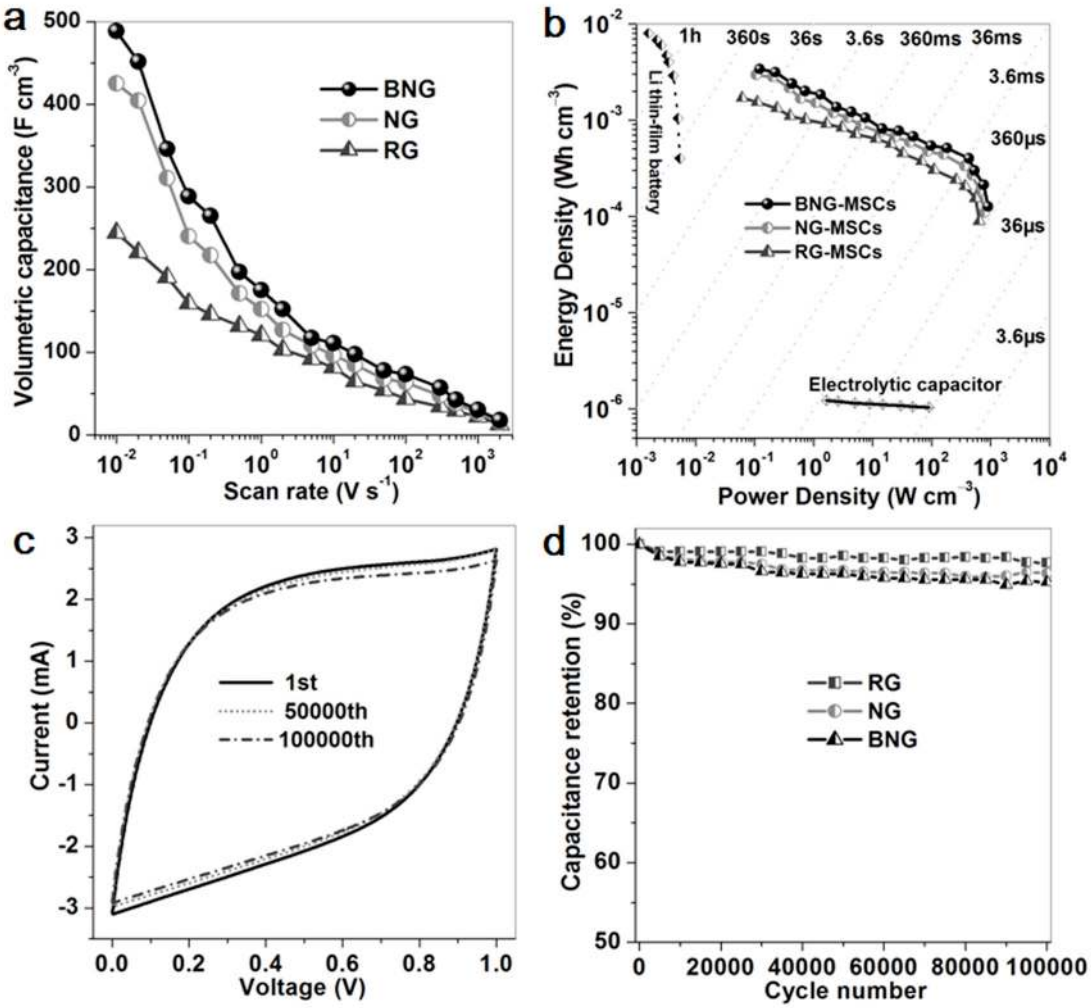

Figure 5. Electrochemical characterization of BNG-MSCs, NG-MSCs, and RG-MSCs. (a) Comparison of the volumetric capacitance of BNG, NG, and RG films for MSCs. (b) Ragone plot of BNG-MSCs, NG-MSCs, and RG-MSCs in comparison with lithium thin-film batteries (4V/500 μAh)[2] and an electrolytic capacitor (3V/300 μF).[31] (c) The 1st, 50000th, and 100000th CV curves of BNG-MSCs measured at 500 V s^{-1}. (d) Cycling stability of BNG-MSCs, NG-MSCs, and RG-MSCs.

The table of contents entry: Highly uniform, ultrathin, layer-by-layer heteroatom (N, B) co-doped graphene films were fabricated for high-performance on-chip planar micro-supercapacitors with an ultrahigh volumetric capacitance of ~488 F/cm^3 and excellent rate capability of 2000 V/s due to the synergistic effect of nitrogen and boron co-doping.

Keyword: Layer-by-layer Self-assembly, Heteroatom Doping, Graphene Film, Energy Storage, Micro-Supercapacitors

***Authors**:* Zhong-Shuai Wu, Khaled Parvez, Andreas Winter, Henning Vieker, Xianjie Liu, Sheng Han, Andrey Turchanin, Xinliang Feng, and Klaus Müllen

Title: Layer-by-layer Assembled Heteroatom-Doped Graphene Films with Ultrahigh Volumetric Capacitance and Rate Capability for Micro-Supercapacitors

ToC figure